CMT Ceramics in Modern Technologies
Techna Group srl



# Functionally Graded Alumina Toughened Zirconia Components made by Ceramic Vat Photo Polymerization (CerAM VPP)

Eric Schwarzer[a]*, Uwe Scheithauer[a], Stefan Holtzhausen[b], Claudia Ortmann[c], Thomas Oberbach[c], Tassilo Moritz[a], Alexander Michaelis[a]
[a]Fraunhofer Institute for Ceramic Technologies and Systems IKTS, Dresden, Germany; [b]Technical University Dresden, Lehrstuhl für Konstruktionstechnik/CAD, Dresden, Germany; [c]Mathys Orthopädie GmbH, Mörsdorf, Germany

Technological progress in the field of additive manufacturing (AM) as a shaping method is inexorably advancing. In particular, AM provides the possibility to manufacture functionally graded components using a voxel model method. In medical technology, especially in implantology, these new structures can open new applications. In order to increase the ingrowth of cells into an implant, a function-optimized structure with a defined porosity gradient seems to be advantageous. In addition, ceramic implants are known for their excellent biocompatibility. From the material side, alumina toughened zirconia is a particularly interesting material. In combination with AM processes, completely new possibilities arise for the production of novel implants. Vat photo polymerization of ceramics (CerAM VPP), also known as lithography-based ceramic manufacturing (LCM), is suitable to realize defined and filigree structures. This article will show results from the process development for CerAM VPP of ATZ components with a defined graded porosity.

*Keywords: Additive manufacturing; Vat photo polymerization of ceramics, CerAM VPP; Lithography-based ceramic manufacturing (LCM); Alumina toughened zirconia (ATZ); Medical implant application; Functionally graded materials (FGM).*

## 1. Introduction

Ceramic materials are known for their excellent properties, like highstrength, chemical resistance, thermal resistance or hardness. Furthermore, medical implants made of ceramics are known for their excellent biological compatibility [1-2]. Caused on the high mechanical strength and biocompatibility, zirconia, especially the yttrium stabilized material, is used as material in biomedical applications [3-4]. However, on the one hand it is known from literature that yttrium stabilized zirconia (YTZP) is susceptible against hydrothermal aging [5-6], on the other hand alumina toughened zirconia (ATZ) shows a higher resistance as compared to YTZP [7-8]. Furthermore, ATZ ceramics combine high wear resistance and hardness of alumina with high mechanical strength of yttrium stabilized tetragonal zirconia polycrystal (YTZP) [9-10]. A promising alternative to conventional shaping technologies for the production of complex parts, especially in the field of ceramics, is given by additive manufacturing. High-complex technical ceramics are increasingly required for many technical applications, also in medical technology. Novel medical implants, for example, must combine different properties in one component. This requirement can be fulfilled by functionally graded materials (FGM). A variety of properties in form of discrete or continuous transitions, like composition gradients or graded porosity in the material [11], can be realized by such FGM. Different studies showed the interconnection between implant material and cells. The ingrowth of cells into an implant, in particular, seems to be advantageous in a function-optimized structure based on a defined pore gradient [12]. An adequate growth of cells was observed for structures with a pore diameter of less than 600 µm. Additive manufacturing technologies offer the possibility to realize such filigree and graded pore structures, because they allows the translation of a computer generated 3D model into a physical product by sequenced addition of material. Stereolithography (SLA) developed by Hull in the 1980s [13] was the first AM technology. Lithography-based ceramic manufacturing (LCM) commercialized by Lithoz [14] (Vienna, Austria) is a further development for ceramic SLA. It allows the production of high-quality ceramics with a mechanical strength comparable to that of standard shaping technologies. According to the terms in the standard (EN ISO/ASTM 52900) and in order to highlight additive manufacturing of ceramics we use the terms “vat photo polymerization of ceramics” or “CerAM VPP” [15] in this article. However, each technology is only as good as the underlying database, especially concerning the required three-dimensional component model. Due to performance limits common CAD systems are not suitable for generating lattice structures which are required to design a 3D-model, e.g. for a new medical implant with a defined porosity of less than 600 $\mu$m or a defined pore gradient. Currently, lattice structures with changing rod geometries or unit cells cannot be sufficiently generated [16-17]. Therefore, a new voxel model approach for the design of components with a defined porosity was developed and tested for CerAM VPP of ATZ components [18]. In this study, further developments of the project “AGENT-3D_FunGeoS“ (03ZZ0208A) concerning the CerAM VPP of ATZ components with a graded porosity designed by the described novel voxel model are presented.

* *Corresponding author*
*E-mail address: eric.schwarzer@ikts.fraunhofer.de*

*https://doi.org/10.29272/cmt.2018.0015*
*Received October 31, 2018; Received in revised form December 19, 2018; Accepted December 28, 2018*

## 2. Materials and Methods

### 2.1. Design of functionally graded structures related to medical implants

The combination of micro- and macrostructures in one component can be a fundamental approach in the field of medical technology. Such a combination can be found in the human femoral bone, for example, consisting of a load-appropriate outer macro-structure with variable cross-section in the cortical bone together with an internal stiffness-variable foam structure in the cancellous bone. These natural structures are highly sophisticated and very interesting for novel patient-specific implants. Additive manufacturing seems to be predestined for shaping such complex designs [19]. Mathys Orthopädie GmbH as a medical supplier defined the general requirements for the ATZ ceramic material, which has to reach bending strength of minimum 500 MPa and a bulk density larger than 5.43 g/cm$^3$. Novel implant structures should have a graded porosity in the range of 200 to 700 µm in pore size with a strut size of approx. 750 µm.

The design of novel structures related to the described specifications was investigated using lattice structure generation based on a voxel model method [27]. With this method, a model of a component was created in a voxel environment by indexing the voxel containing material as "empty" or as "filled". The proportion of the design results from the component cartesian bounding box and a previously defined, problem-specific voxel size. Unit cell-based geometry models derived from their individual parts like rod geometries and nodes, which are convertible into a voxel model, are the basis of this method. The size of the elements, especially the ball diameter of the unit cell nodes can be specified globally or adjusted locally by means of a density field. Moving and rotating these voxel models and overwriting the values in the global component voxel model, the lattice structure increases piece by piece. The advantage of this method is that computationally intensive incision operations of the individual cells for a consistent mesh model are not necessary. Within a component, the lattice structure geometry can be easily changed and recalculated. It is also possible to create non-regular structures. The use of three-dimensional filter matrices, equivalent to 2D image processing, is an effective way of smoothing, thickening or thinning the data. A more detailed description of the method and the design of first novel lattice structures with a defined porosity is given in a previous publication [18].

This study presents the further development from a non-graded defined porosity [18] (old design) to a model with a defined graded porosity (new design). Figure 1 shows a comparison between the "old" and the "new" design.

The specification of the "new" model concerning the inner graded porosity was based on the usual conditions for medical implant components. Pore sizes in a range of approx. 300 µm to 700 µm were defined for the whole component design, because this seems to ensure the ingrowth of cells.

Similar to the "old" design, the subtracting method was used to create a design with graded porosity, whereby defined cavities created the pattern. These drop-shaped cavities were created using a defined rod geometry. A corresponding profile was selected between the rod nodes and the extrudes. The profile

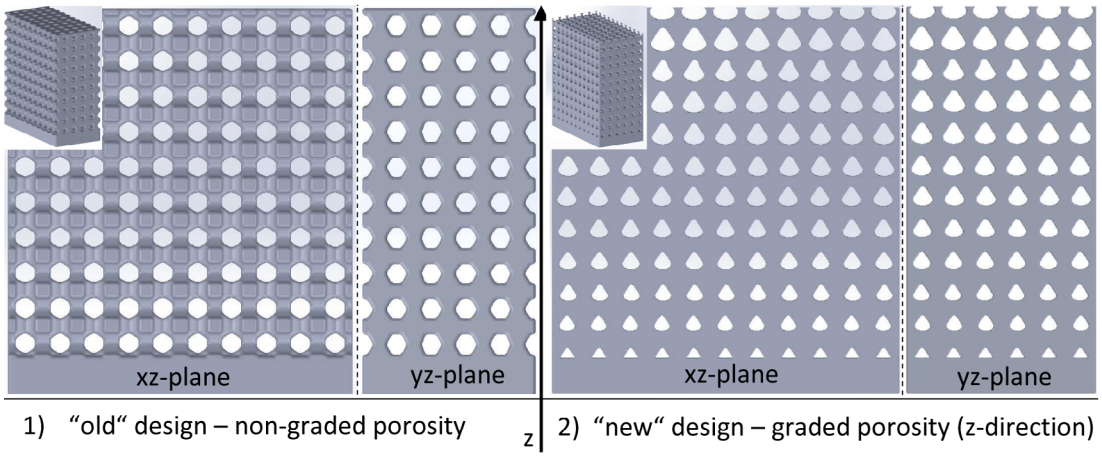


*Figure 1. Old design (1) [18] compared to the "new" design (2); further development with graded porosity.*

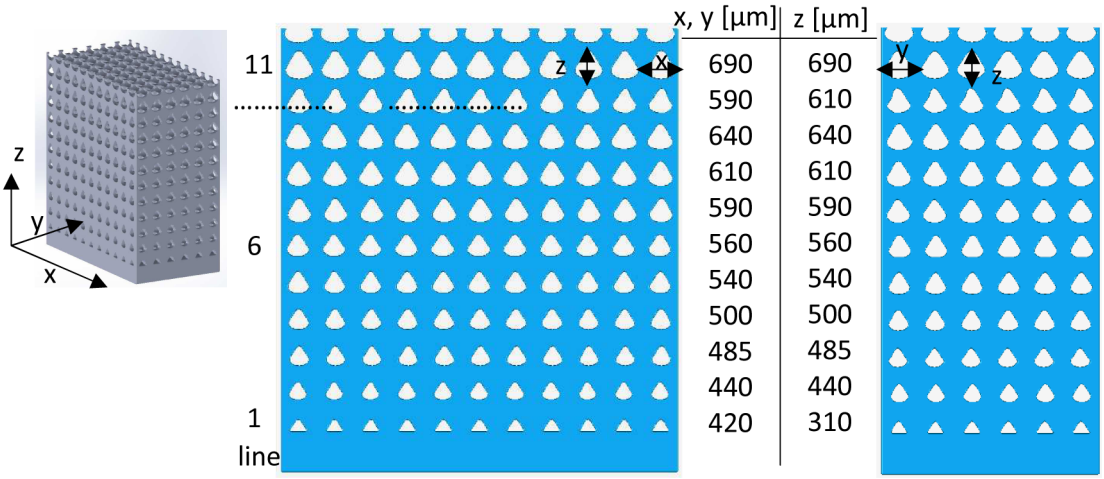


*Figure 2. Graded porosity of the "new" design and its dimensions in different directions.*

itself was normalized, i.e. it lies within a rectangular cross-section of size one. By specifying a location-dependent size, the profile was scaled accordingly in each node. Graded profiles were created, which were subtracted from the envelope geometry. The advantage of this drop-shaped profile was that critical and too flat angles in the direction of construction were avoided. In comparison, the profile was installed with 90 degrees rotation in the yz-plane.
Figure 2 shows the different sides of the "new" lattice structure component with graded porosity and their cavity dimensions, which were used to compare the dimensional target accuracy with the printed components in the green and sintered state.

*2.2. Vat photo polymerization of ceramics (CerAM VPP)*

Despite the currently hype, the variety of commercially available AM methods for high-quality technical ceramics is relatively small. One potential technology is vat photo polymerization of ceramics (CerAM VPP), which was commercialized as the lithography-based ceramic manufacturing (LCM) process by Lithoz GmbH. It is an enhancement of the digital light processing (DLP) technology for the production of high-performance ceramics. With the CeraFab7500 device, a printer of high resolution (635 dpi; 40 µm pixel-size; 5-100 µm layer thickness) for AM of high quality ceramics with a material density higher than 99% of the theoretical density is available [14]. The technology is based on a photoreactive suspension curable by photons coming from a special light source (wavelength 452-465 nm; intensity 30-55 mW/cm$^2$) [14, 20, 21]. Due to an adjustable rotating vat (diameter of 15 cm), usual upcoming shear rates within the process are up to approx. 300 s$^{-1}$ (doctor blade gap of approx. 175-500 µm) as a significant parameter influencing the rheological behaviour of suspensions. This should be kept in mind for their development. Detailed descriptions have been published in various articles [15, 22-26]. Considering the described aspects, a novel ATZ suspension was developed and different test components were printed for validation by using the Lithoz device [18]. In this study, new results for the printing of novel lattice structures with a graded porosity as well as an improvement of mechanical properties of a printed ATZ material are presented.

*2.3. Additive manufacturing using CerAM VPP*

*2.3.1. CerAM VPP of ATZ-components*

Related to the material requirements described above, a suspension with a solid content of approx. 47 vol.% (82 wt.%) based on an ATZ ceramic powder (Mathys Orthopädie GmbH) with a narrow particle size distribution, a mean particle size < 0.5 µm and a specific surface of approx. 7.5 m$^2$/g was used for the CerAM VPP process. The photoreactive resin composition was a mixture of a monomer acrylate (4 hydroxybutylacrylate, BASF) and two different multifunctional crosslinker – a difunctional acrylate (3-methyl-1,5 pentanediol diacrylate, IGM resins) and a tetra-functional polyol acrylate (Ebecryl 40, Allnex). The ratio between the crosslinker and the monomer acrylate was 1.2, with a ratio of 0.65 between the di- and tetrafunctional crosslinker. With an amount of 1.25 wt.% related to the photoreactive organic, camphorquinone as type II initiator was used in combination with ethyl 4-(dimethylamino)benzoate as co-initiator, because they are known for activation at visible light, e.g. at wavelengths of 445-465 nm. Additionally, a long chain polyethylenglycol was added as plasticizer in a share of 30 wt.% related to the reactive organics. The ATZ powder was homogeneously dispersed in the photoreactive resin composition by using a high-speed vacuum planetary mixer (Thinky ARV 310, C3-Prozesstechnik, Germany, Ltd.) for 3 minutes at a rotation speed of 2000 rpm. The suspension development has already been described in a previous study [18]. The suspension preparation started with the processing of the ATZ powder by deagglomeration in a planetary ball mill (Pulverisette, Fritsch Ltd.) for 2 h at 230 rpm. Therefore, the ATZ powder (approx. 70 wt.%) was mixed together with a volatile solvent (approx. 30 wt.%) such as ethanol or isopropyl, 1 wt.% dispersant (BYK LP C22124, BYK-Chemie, Ltd.) related to the solid content and mill balls in the same absolute mass ratio as compared to the powder content. By using a sieve, the mill balls were removed after the processing and the powder was dried in a fume hood for 12 h followed by a drying chamber at 110 °C for 24 h. The prepared ATZ powder were characterized concerning the particle size distribution (PSD) by laser diffraction method (Mastersizer 2000, Malvern Instruments Ltd., United Kingdom) and the particle shape by FESEM analyses (Gemini 982, Zeiss Ltd., Germany) analyses.
After drying, the prepared powder was mixed to a homogeneous suspension together with different organic components by using a high-speed vacuum planetary mixer (Thinky ARV 310, C3-Prozesstechnik, Germany, Ltd.).
The prepared suspension was used for CerAM VPP of test components – cuboidal plates (20x20x2 mm; green size) and the "new" lattice structure component. During the sintering of ceramics, a material- and process-specific shrinkage occurs which has to be considered for the printing process. For that reason, correction factors have to be used as an upscaling in each dimension. The correction factors for the used ATZ suspension in x, y and z-direction were previously determined with a factor of 1.26 for the xy-direction and a factor of 1.285 for the z direction [18]. These factors were used as scaling factors directly in the printer device software. The dimensions of the lattice structure cavities were enlarged by the estimated oversize factors to achieve the correct dimensions after sintering. Possible anisotropic material properties, e.g. the strength, are based on the layerwise building process. Therefore, the orientation of the components on the building platform can have a decisive influence to the final material properties. Due to this fact, the narrow side of the cuboidal plates with 20 mm (y-direction) and 2 mm (x-direction) edge lengths built the base area connected to the building platform during the print. The plate length of 20 mm was printed in building direction (z-direction) by creation of 800 layers (25 µm layer thickness). The lowest strength values were expected for printing the plates by the described orientation, caused to the parallelism of the interconnection zones between the layers and the force transmission within the biaxial strength test. After printing, all test samples were cleaned by using pressured air and a special cleaning solvent (Lithasol) from Lithoz.

*2.3.2. Characterization and thermal processing*

Directly after cleaning the printed green components were characterized regarding their dimensions, cracks and printing quality by using digital light microscopy and a digital caliper. By means of a microscope, on the one hand the component surfaces were checked for cracks and defects. On the other hand, the dimensions of the cavities in x, y and z direction for each side (xz-plane and yz-plane) of the lattice structure component were determined, both exemplarily shown in Figure 3.
The average value of the cavity dimension per line of each side was calculated and compared to the target value. By this result, the resolution and the printing quality as well as the cleaning process were assessed.
After characterization, the printed green components were thermally treated in two consecutive steps comparable to the standard ceramic processing steps of debinding and sintering. For the thermal processing, the CerAM VPP components were placed on a special kiln furniture, which was sintered at a temperature at least 50 K higher as compared to the final sintering temperature of the printed components. For this reason, a transfer of the debinded components to another kiln furniture is not necessary. Based on a previous thermogravimetric analyse, a heating profile

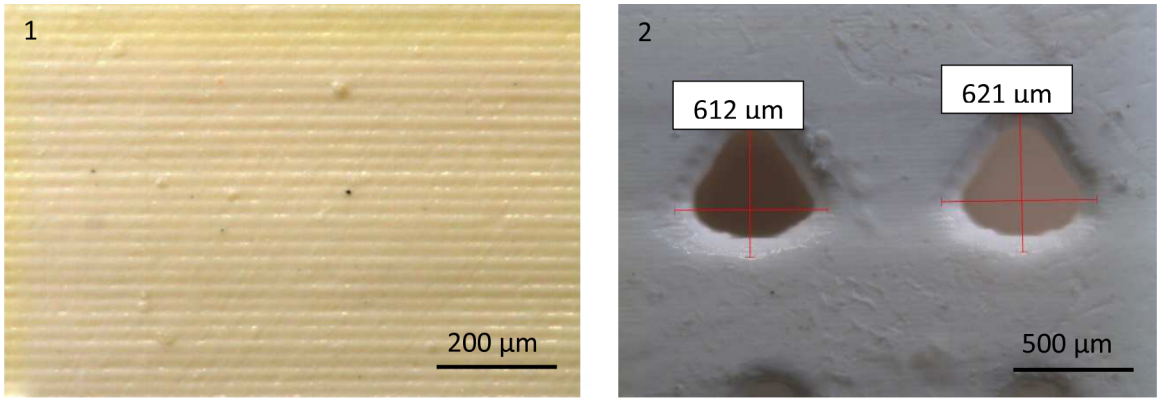


*Figure 3. Microscopic image – cuboidal plate (1) and "new" lattice structure component (2).*

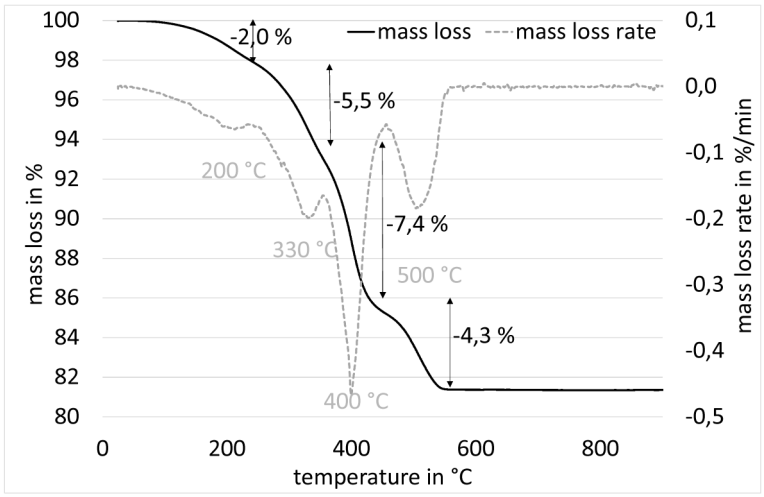


*Figure 4. Thermogravimetric analyse; mass loss (black) and mass loss rate (dashed grey) in dependence to temperature.*

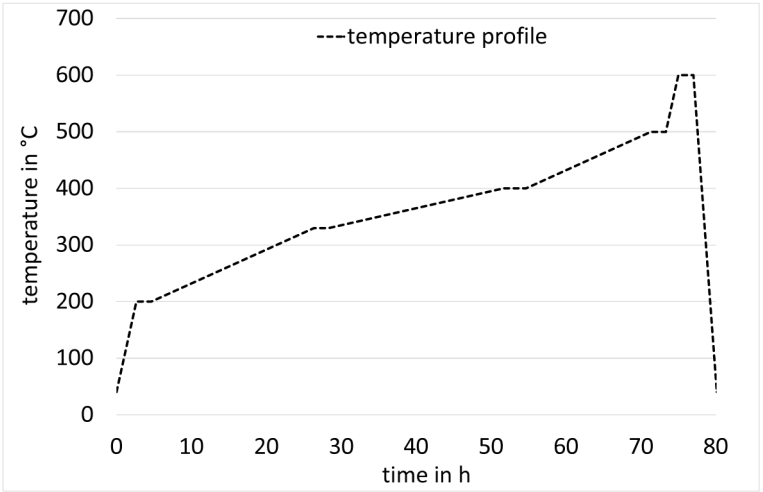


*Figure 5. Temperature profile for debinding of ATZ components in air atmosphere derived from thermogravimetric analyses.*

was calculated as basis for the debinding step. The result of the thermogravimetric analyses is presented in Figure 4 by showing the mass loss as well as the mass loss rate in dependence to temperature. The heating rate was of 3 K/min up to 900 °C as end temperature.

Four significant peak points were identified based on the thermogravimetric analyse. Up to 200 °C as first peak point, the mass decreased by 2%, as an indicator for the loss of plasticizer. The second peak point was at approx. 330 °C. In the range of 250 ° C and 360 °C the mass decreased by 5.5%. In the range of 360 °C and 450 °C, the mass decreased by approx. 7.4% with a third peek point at 400 °C. A fourth peak point was identified at 500 °C, with a mass loss of 4.3 % in the range of 450 °C to 520 °C. The total mass loss was approx. 19 %, complementary to the organic amount of the suspension. Based on this analyse, a debinding profile was derived, shown in Figure 5.

Sintering was done in another sintering furnace (LH 15/12, Nabertherm, Germany) under air with a heating rate of 2 K/min up to 1500 °C with 2 h dwell-time, a set-up given by Mathys Orthopädie GmbH. In order to eliminate residual pores in the microstructure leading to an increase of the material strength, the sintered components were densified in an additional step by hot isostatic pressing (HIP) at 1450 °C with a pressure of 1000 bar for 2 h.

The components were characterized after sintering regarding shrinkage, dimensions, density, structure, defects and strength. The density was calculated by Archimedean method by measuring the dry mass, the wet mass and the mass in water depending on the material-specific buoyancy by using a special gauge setup (KERN ABS-N/ABJ-NM + EMB 200-3V, Kern, Germany, Ltd.).

By using digital light microscopy, the lattice structure components with graded porosity were randomly analysed in terms of defects, quality and delamination as well as the dimensions of the cavities – same workflow as described above for green components. Information about the sintered ATZ material strength was determined on the basis of cuboidal plates by measuring the biaxial strength related to Danzer´s "ball-on-three-balls" method [28]. This method is usually validated for circular samples, but it is also described that the influence of the geometry can be neglected.

## 3. Results and Discussion

According to the requirements of Mathys Orthopädie GmbH, a high material density (>99%) and an as high as possible mechanical strength (>500 MPa) of the ATZ material are necessary to pass the applicable medical device testing standards. The measured particle size distribution (PSD) of the ATZ powder and a FESEM view of the used powder are presented in Figure 6. By deagglomeration of the powder in the described manner, a well prepared ATZ material was achieved, because of the determined narrow PSD. The mean particle size (d50) is approx. 0.5 µm and 90% (d90) of the particles were smaller than approx.

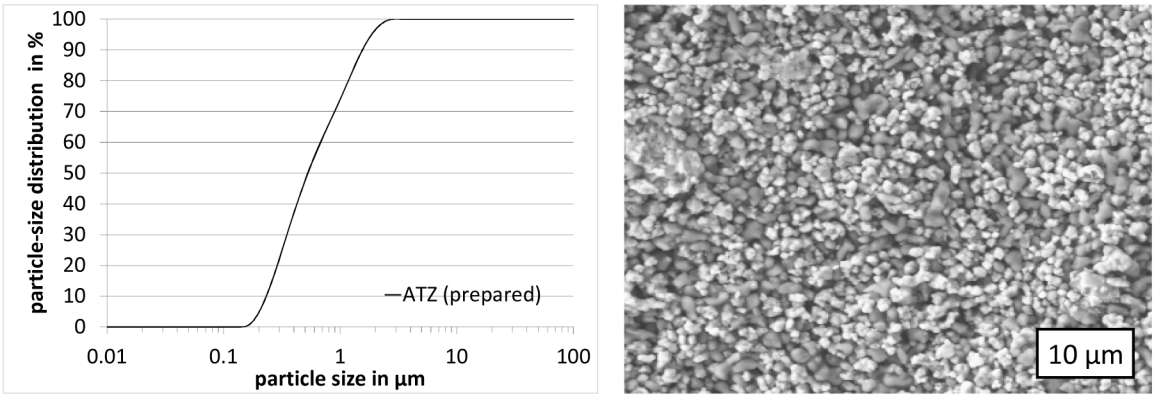


*Figure 6. PSD (1) and FESEM (2) image of the prepared ATZ material.*

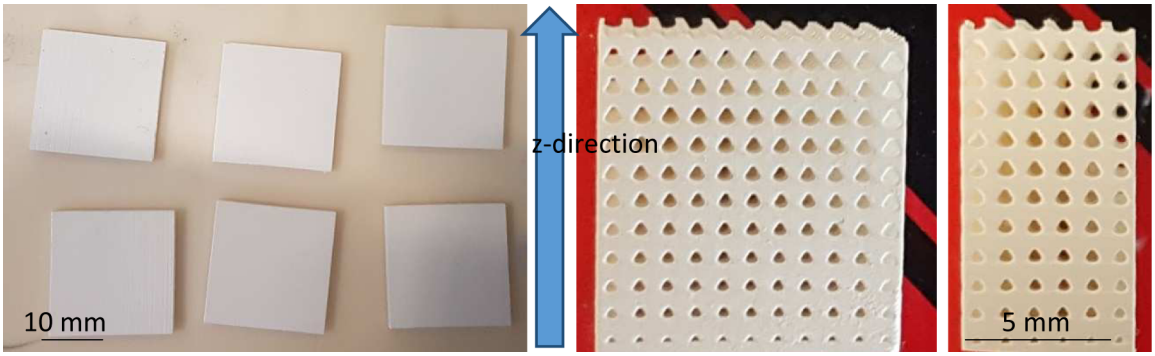


*Figure 7. CerAM VPP cuboidal plates (1) and a "new" lattice structure component with graded porosity (2); green state.*

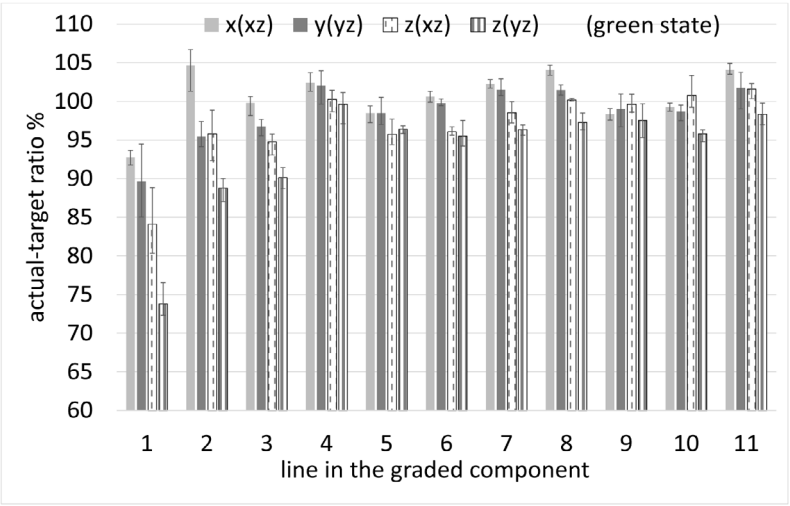


*Figure 8. Accuracy of the cavity dimensions for the lattice structure component as actual-target ratio (green state).*

1.7 µm, good prerequisites for the CerAM VPP process and the production of high-quality sintered ceramic. The FESEM image also shows a very homogeneous powder with particle shapes that are standard for a well-dispersed material.

The photoreactive suspension with the well-dispersed ATZ material was used for the CerAM VPP of the cuboidal plates and the "new" lattice structure component with a pore gradient in z-direction. A selection of the printed components (green state) is exemplarily shown in Figure 7.

The CerAM VPP cuboidal plates and the "new" lattice structure components show a sufficient quality after cleaning, no cracks or delamination were determined and the green strength was high enough for handling and characterizations.

Based on the orientation of the lattice structure component with graded porosity shown in Figure 2, in every line the length of largest dimension of the cavities in x and z for the xz-side and in y and z for the yz-side were determined and then compared to the given target values. Due to the use of oversize factors (correction factor) the dimension of the cavities in the green state were enlarged to compensate the sinter shrinkage. The specified target dimensions had to be increased by the correction factors in the respective direction before they were compared with the measured green dimensions of the lattice structure components. The comparison was made as percentage ratio of the measured dimensions (green state) to the oversized target dimension. The result is summarized in Figure 8 as bar chart by plotting the calculated percentage ratio between the actual and target value for both sides (xz-side and yz-side) in dependence to the line (1 to 11).

In that case hundred percentage means a perfect match, whereby smaller values indicated smaller dimensions. The error bars show the complete range between the minimum and maximum of the dimension measurements per line. In general, the accuracy of the lattice structure component cavities shows a good match to the theoretical target value. Excluding the first row, values in a range of approx. 95% to 105% for the x- and y-dimensions were achieved. This is a very good result. In that case, the high resolution of the CerAM VPP process was nearly perfectly used. In line "1" the deviation is higher and an accuracy of 90% to 94% was determined, which seems to be suboptimal at first glance. But it should be remembered that the resolution of the used AM device is 40 µm in the xy-direction. Thus, one pixel has a dimension of 10% in contrast to the target dimension of approx. 400 µm. Only one pixel at every edge in one direction influences the target accuracy up to 20%. Such deviations were based on the process itself, for example on adherent suspension or a kind

of scattering effect, and are difficult to control. The phenomenon of overexposure is well known [22]. With respect to this fact, the accuracy is still good. For the dimension in z-direction the result was a bit different. Excluding the first row, the accuracy for the z-dimensions is comparable to the xy-dimension with marginally smaller values. However, in the "1" line the accuracy was in a range of 74% to 85%, significantly lower as compared to the xy-dimensions. This might be caused by the very small cavities in combination with light scattering effects and the exposure of adherent suspension within the cavity, which could not be removed by cleaning.

The characterized lattice structures components were debindered and sintered together with the cuboidal plates in the same treatment. After sintering and hot isostatic pressing of the cuboidal plates, a further characterization was done.

The density of the ATZ material directly measured after sintering had an average value of approx. 5.45 g/cm³. By hot isostatic pressing, it was possible to increase the density up to an average value of approx. 5.49 g/cm³, larger than 99.5% related the theoretical ATZ material density of 5.51 gcm³. The biaxial strength of the hot isostatically pressed ATZ was determined by ball-on-three-ball method. The results are presented in Figure 9 and compared to conventional isostatically pressed ATZ and sintered additive manufactured ATZ components without HIP from a previous measurement [17].

By hot isostatic pressing, the biaxial strength of the ATZ was significantly increased to an average of 900 MPa which is more than two times higher as compared to the ATZ without HIP – and 90% of the isostatically pressed ATZ strength. Hot isostatic pressing significantly reduced the porosity as defect initiator, marked by an increase of the density, resulting in a decreased defect susceptibility.

In Figure 10, a sintered lattice structure component with a graded porosity is exemplarily presented in total view and in detail by a microscope image.

Sintering of the lattice structures were successful, because no bigger defects, crack or delamination became visible. The filigree struts of the different planes and between the different lines seem to be well connected and the whole components were of high strength. Neither the microscope (Figure 8) nor the computer tomography showed any cracks or defects. The strength of the lattice components will be tested in the future.

After sintering, the dimensions of the component cavities were measured again and the results are summarized in Figure 11, similar to the green characterization. The calculated ratio between the measured (actual) and the theoretical (target) dimensions in dependence to line and side is presented for accuracy rating.

As for the characterization in the green state, the accuracy of the lattice structure component cavities shows a good match to the theoretical target value. Excluding the first row similar to the characterization in the green state, values in a range of approx. 93% to 103% for the x- and y-dimensions were achieved. For

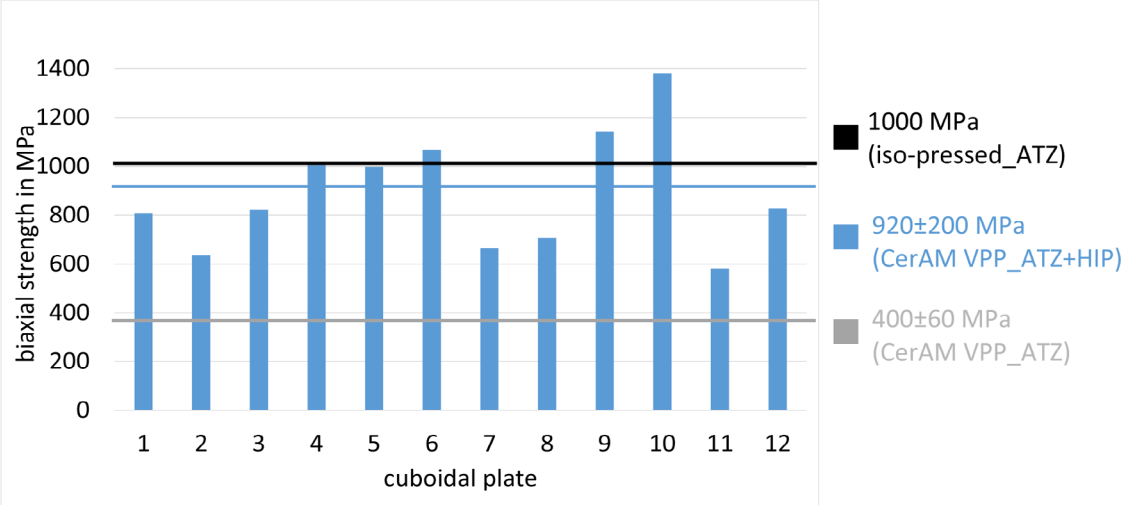


*Figure 9. Biaxial strength of the cuboidal ATZ material additively manufactured by CerAM VPP and densified by HIP.*

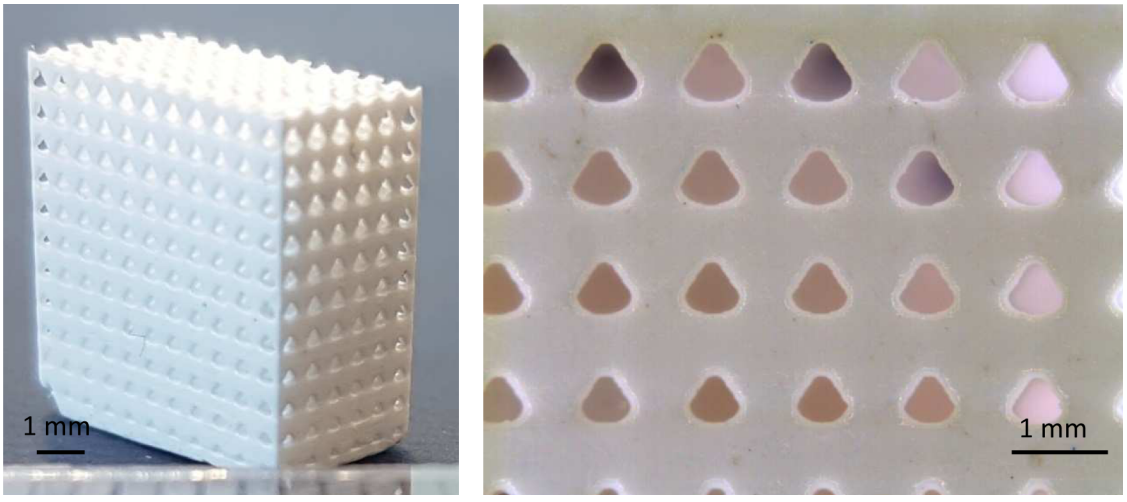


*Figure 10. Sintered part of a "new" lattice structure component, total view (1) and a microscopic image (2).*

line "1", the accuracy is approx. 85%, the same deviation as in the green state. The dimension in z-direction ranged also in values of approx. 87% to 97%, comparable to the green state. The differences between the z dimension in line "1" for the two sides were also found in the sintered state. Due to that fact, a larger measurement error was excluded. This aspect has to be investigated more in detail. Due to similar trends in the green and sintered state, the previous determination of the printing correction factors seems to be correct.

Figure 12 presents FESEM images of sintered ATZ ceramics made by CerAM VPP. They show the microstructure and the grain size of the material, which are indicators for the quality of the whole development.

The FESEM images show very homogeneous ATZ microstructures with a homogeneous grain size distribution. Larger defects or pores were not found. All three phases – zirconia (1), alumina

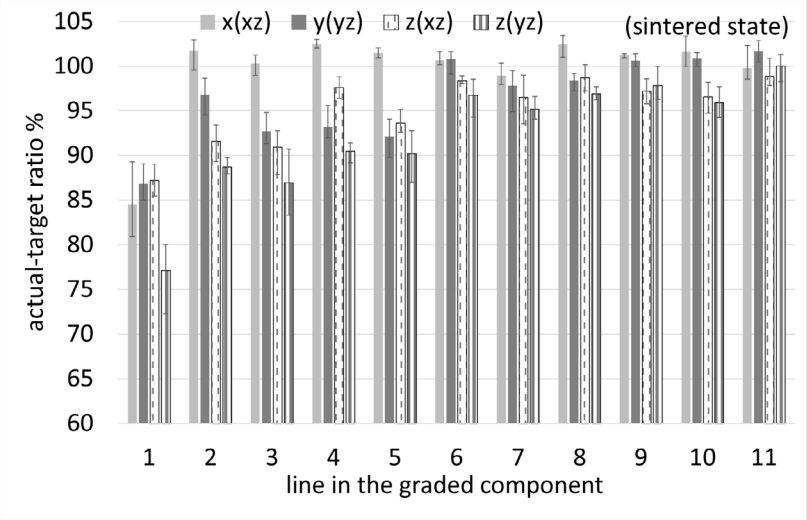


*Figure 11. Accuracy of the cavity dimensions for the lattice structure component as actual-target ratio (sintered state).*

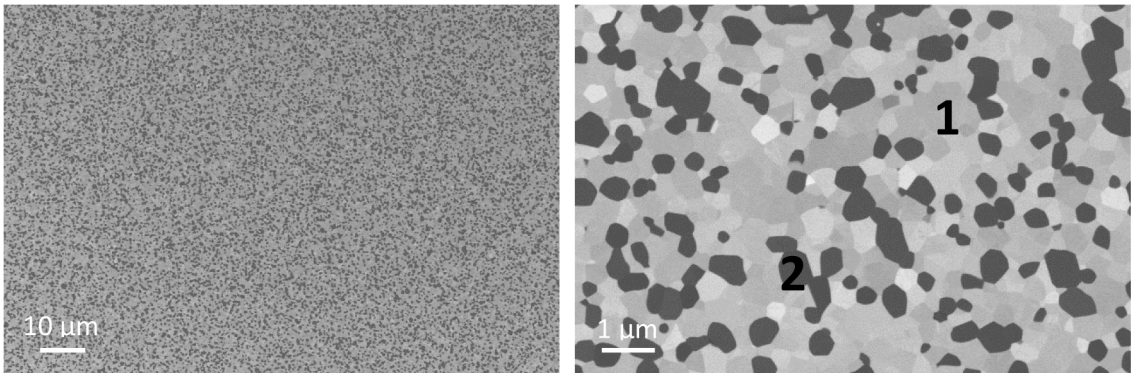


*Figure 12. FESEM images of a sintered ATZ structure made by CerAM VPP with zirconia (1) and alumina (2) phases.*

(2) and yttria – were homogeneously distributed and had been detected by energy-dispersive X-ray spectroscopy. During the analyses, the yttria phase was always found in combination with the zirconia phase, but a distinction in the FESEM image was not possible. In general, the grain sizes were smaller than one micron, which indicates a sufficient distribution and deagglomeration of the particles.

## 4. Conclusion

Alumina toughened zirconia is an interesting ceramic material for future of implants, because it combines high wear resistance and hardness of alumina with high mechanical strength of YTZP. The combination of these properties with lattice structure generation provides the possibility to design completely new ATZ components using AM technologies. This enables many new applications, especially in medical technology.

Based on an innovative voxel model method, new functionally graded components with a graded porosity were designed and manufactured by using CerAM VPP.

The components were manufactured by using a photoreactive suspension based on an ATZ material, which was developed and validated in a previous study. For the lattice structure components with graded porosity, a good accuracy of the cavities between the measured dimensions and the target dimensions of the digital model were determined. The accuracy of the dimensions was in a range of approx. 95 % to 105 % as compared to the theoretical values.

By hot isostatic pressing, the density and the biaxial strength of the printed ATZ components were significantly increased. The values can be compared to those of conventionally manufactured ATZ materials. FESEM analyses showed a homogeneous micro structure with a homogeneous and narrow grain size distribution without any larger defects or pores. Based on the development, it is possible to realize complex ATZ components of high accuracy and with advanced ceramic properties by CerAM VPP.

## Acknowledgement

Financial funding of this project "AGENT-3D_FunGeoS" from the German Federal Ministry of Education and Research under the grant number 03ZZ0208A is gratefully acknowledged. The responsibility for the content of this publication lies with the author.

## References

[1] B. Möller, H. Terheyden, Y. Acil, N.M. Purcz, K. Hertrampf, A. Tabakov, E. Behrens, J. Wiltfang, A comparison of biocompatibility and osseointegration of ceramic and titanium implants: an in vivo and in vitro study" Int. J. Oral maxillofac Surg., 41(5), pp. 638-45, DOI: 10.1016/j.ijom.2012.02.004., (2012).

[2] A. Afzal, Implantable zirconia bioceramics for bone repair and replacement: A chronological review, Mater. Express, Vol. 5, No. 1 (2014).
[3] A. Eichler, Tetragonal Y-doped zirconia: structure and ion conductivity, Phys. Rev. B 6, 174103 (2001).
[4] S. Shukla and S. Seal, Mechanism of room temperature metastable tetragonal phase stabilistaion in zirconia, Int, Mater. Rev. 50, 45, (2005).
[5] R. Dittmann, E. Mecher, A. Schmalzl, T. Kuretzky, Effect of hydrothermal aging on zirconia crystal phases and strength, Dental Materials, Vol. 26 (1), pp. e49-e50, DOI: https://doi.org/10.1016/j.dental.2010.08.113, (2010).
[6] E.M. Munoz, D. Longhini, S.G. Antonio, G.L. Adabo, The effects of mechanical and hydrothermal aging on microstructure and biaxial flexural strength of an anterior and a posterior monolithic zirconia, Journal of Density, Vol. 63, pp. 94-102, (2017).
[7] S. Begand et al., Kinetic of the phase transformation of ATZ compared to biograde Y-TZP, Key Engineering Materials, Trans. Tech. Publ., (2008).
[8] J. Chevalier, B. Cales, J.M. Drouin, Low Temperature Ageing of Y-TZP Ceramics, Journal of American Ceramic Society 82, 2150-2154, (1999).
[9] M. Al-Hajjar et al., Wear of novel ceramic-on-ceramic bearings under adverse and clinically relevant hip simulator conditions, J. Biomed. Mater. Res. B. Appl. Biomater., (2014)
[10] S. Begand, et al., ATZ - A new material with a high potential in joint replacement, Key Eng. Mater. 284-286: pp. 983-986, (2005).
[11] B. Möller, H. Terheyden, Y. Acil, N.M. Purcz, K. Hertrampf, A. Tabakov, E. Behrens, J. Wiltfang, A comparison of biocompatibility and osseointegration of ceramic and titanium implants: an in vivo and in vitro study, Int. J. Oral maxillofac Surg., 41(5), pp. 638-45, (2012), DOI: 10.1016/j.ijom.2012.02.004.
[12] R.R. Felicity, L.A. Cyster, D.M. Grant, C.A Scotchford, S.M. Howdle and K.M. Shakesheff, In vitro assessment of cell penetration into porous hydroxyapatite scaffolds with a central aligned channel, Biomaterials 25, p. 5507-5514, (2004).
[13] C.W. Hull, Apparatus for production of three-dimensional objects by stereolithography, (1984), Patent US4575330B1.
[14] J. Homa, Rapid Prototyping of high-performance ceramics opens new opportunities for the CIM industry, Powder Injection Moulding International, 6 (3), 65-68, (2012).
[15] U. Scheithauer, S. Weingarten, J. Abel, E. Schwarzer, W. Beckert, H.-J. Richter, T. Moritz, A. Michaelis, Additive Manufacturing of Ceramic Based Functionally Graded Materials, Ceramic Applications, 6, 30-36, (2018).
[16] R.M. Gorguluarslan, U.N. Gandhi, R. Mandapati, S.-K. Choi, Design and fabrication of periodic lattice-based cellular structures. Computer-Aided Design and Applications, 13, 50-62, (2015).
[17] O. Rehme, C. Emmelmann, Rapid manufacturing of lattice structures with selective laser melting. In F.G. Bachmann, W. Hoving, Y. Lu, & K. Washio (Hrsg.), Lasers and Applications in Science and Engineering (S. 61070K). SPIE, (2016).
[18] E. Schwarzer, S. Holtzhausen, U. Scheithauer, C. Ortmann, T. Oberbach, T. Moritz, A. Michaelis, Process development for additive manufacturing of functionally graded alumina toughened zirconia components intended for medical implant application, article in press, J. Europ. Ceram. Soc., (2018), https://doi.org/10.1016/j.jeurceramsoc.2018.09.003
[19] L.J. Gibson, Biomechanics of cellular solids, Journal of Biomechanics, 38, 377–399, (2005).
[20] U. Scheithauer, S. Weingarten, R. Johne, E. Schwarzer, J. Abel, H.-J. Richter, T. Moritz and A. Michaelis, Ceramic-Based 4D Components: Additive Manufacturing (AM) of Ceramic-Based Functionally Graded Materials (FGM) by Thermoplastic 3D Printing (T3DP), Materials, 10 (12), 1368; doi:10.3390/ma10121368, (2017)
[21] U.K. Fischer, N. Moszner, V. Rheinberger, W. Wachter, J. Homa, W. Längle, Lichthärtende Keramikschlicker für die stereolithographische Herstellung von hochfesten Keramiken, EP 2 404 590 A1 (2012).
[22] G. Mitteramskogler, R. Gmeiner, R. Felzmann, S. Gruber, C. Hofstetter and J. Stampfl, Light curing strategies for lithography-based additive manufacturing of customized ceramics, Additive Manufacturing 1-4, pp. 110–118, DOI: 10.1016/j.addma.2014.08.003c, (2014).
[23] J. Ebert, J. Homa, et al., Verfahren zum schichtweisen Aufbau eines Formkörpers aus hochviskosem photopolymerisierbarem Material, EP 2 505341 B 1, (2011).
[24] U. Scheithauer, E. Schwarzer, G. Ganzer, A. Körnig, W. Beckert, E. Reichelt, M. Jahn, A. Härtel, H.-J. Richter, T. Moritz, A. Michaelis, Micro-reactors made by lithography-based ceramic manufacturing (LCM), in: Proceedings of 11th International Conference on Ceramic Materials and Components for Energy and Environmental Applications 2015, Vancouver, Ceramic Transactions, 258,The American Ceramic Society, (2016).
[25] U. Scheithauer E. Schwarzer T. Moritz, A. Michaelis, Opportunities and limits of the Lithography-based Ceramic Manufacturing (LCM), Journal of Materials Engineering and Performance, 27(1), 14-20, (2018).
[26] E. Johansson, O. Lidström, J. Johansson, O. Lyckfeldt, E. Adolfsson, Influence of Resin Composition on the Defect Formation in Alumina Manufactured by Stereolithography, In Materials, 10, 138, (2017) DOI:10.3390/ma100020138.
[27] V. Chandru, S. Manohar, C.E. Prakash, Voxel-based modeling for layered manufacturing. IEEE Computer Graphics and Applications, 15, 42-47, (1995).
[28] R. Danzer, W. Harrer, P. Supancic, T. Lube, Z. Wang, A. Börger, The ball on three balls test – Strength and failure analysis of different materials, J. Europ. Ceram. Soc., 27, 1481-1485, (2007).